

Deformation of the Upper and Lower Surfaces of an Airfoil by Macro Fiber Composite Actuators

Marco Debiasi^{1,§}, Yann Bouremel², and Zhenbo Lu³
Temasek Laboratories, National University of Singapore, Singapore, 117411

Varsha Ravichandran⁴
School of Mechanical & Aerospace Engineering, Nanyang Technological University, Singapore, 639798

In this follow-on study, macro fiber composite actuators were used to change the shape of the upper and lower surfaces of an airfoil model with geometry close to that of a NACA 0014. In the design discussed, these thin and light piezoelectric actuators are bonded to the inside and become an integral part of the skin of the upper and lower surfaces of the airfoil. Still-air and wind-tunnel measurements in different flow regimes were performed to assess the characteristics of the static changes of the shape of the airfoil. The results obtained can be used to design a wing with morphing surfaces for improving its aerodynamics, for maneuvering without ailerons, and/or for active control of the flow over the wing.

Nomenclature

c	=	model chord
C_D	=	drag coefficient
C_L	=	lift coefficient
C_M	=	pitching-moment coefficient about $c/4$
D	=	drag force
L	=	lift force
l	=	local coordinate tangent to the airfoil surface
n	=	local coordinate normal to the airfoil surface
Re_c	=	Reynolds number based on the chord
s	=	model span (from wall to wall of the wind tunnel)
U	=	flow velocity
x	=	streamwise coordinate of the wind tunnel
y	=	spanwise coordinate of the wind tunnel
z	=	vertical coordinate of the wind tunnel

Greek letters

α	=	angle of attack of the airfoil
ξ	=	axial (chordwise) coordinate of the airfoil
ζ	=	normal coordinate of the airfoil

Subscripts

cp	=	center of pressure
∞	=	freestream conditions

¹ Senior Research Scientist, Temasek Laboratories, National University of Singapore, Singapore, Member AIAA.

² Research Scientist, Temasek Laboratories, National University of Singapore, Singapore, Member AIAA.

³ Research Scientist, Temasek Laboratories, National University of Singapore, Singapore.

⁴ Graduate Student, School of Mechanical & Aerospace Engineering, Nanyang Technological University, Singapore.

I. Introduction

THE ability to change the shape of a wing allows adapting it to different flight conditions. Birds and bats have developed through evolution wings capable of dramatic and continuous morphing not only for generating the lift required to stay aloft, but also to propel themselves in the air and to perform controlled maneuvers. To a smaller extent the wings of aircraft can also achieve discrete changes of their shape by using ailerons, flaps, and slats or by modifying their sweep, dihedral, or incidence angle. Thus much research is devoted to understand and optimize extensive types of wing morphing for improving the aircraft performance.¹⁻⁶ However, extensive wing morphing poses significant design challenges and requires complex mechanical structures and actuators. By contrast limited but smooth morphing of a wing can often be sufficient for the needs of flight (as shown by the minimal movements of the wings of various birds in some flight conditions). The selective displacement of an airfoil upper surface by less than 0.5 % of its chord is sufficient to introduce changes of the pressure distribution useful for tailoring the lift and drag coefficients at high-subsonic speed.⁷ This can be used to optimize the performance of an airfoil around a design point, for instance at cruise conditions. Asymmetric changes in the left and right wing can also be used to maneuver an aircraft without using ailerons. Larger displacements would be required at lower speed, but still within a few percent of a wing chord. Furthermore, limited shape changes appear more feasible for actuation at high frequencies.⁸ This can be exploited to actively control some undesirable phenomena of the wings like flow separation⁹⁻¹¹ and aeroelastic oscillations.¹²⁻¹⁴

A major difficulty in implementing wing morphing is represented by the size, weight, complexity, and power¹⁵ demanded by the appropriate actuators (hydraulic, pneumatic, electric motors, or even some smart materials like shape-memory alloys). From a system-integration point of view, the performance increase offered by the morphing must outweigh its associated penalties. In this respect, limited morphing is also appealing as it may offer useful aerodynamic advantages with small, light, simple, and power-saving actuators.

The macro fiber composite (MFC) actuators, originally developed at NASA, belong to this category and seem promising for implementing different types of wing morphing, especially if limited shape changes are required. These thin, light, and flexible piezoelectric actuators, Fig. 1, consist of rectangular piezo-ceramic rods sandwiched between layers of adhesive and electroded polyimide film which contains interdigitated electrodes that transfer the applied voltage directly to the rods. When embedded in a surface or attached to flexible structures, the MFCs provide distributed deflection and vibration control. They can also be used as sensors to measure the structural strain under applied loads.

Some studies have explored the use of such actuators to change or control the shape of aerodynamic bodies. Munday et al. used THUNDER actuators (a predecessor of the MFC type, also developed at NASA) to increase the lift of an airfoil.⁹⁻¹¹ Their morphing airfoil model is based on a prototype made by Pinkerton and Moses.¹⁶ Static and dynamic morphing tests were conducted at angles of attack from 0° to 9° at low Reynolds numbers of $2.5 \cdot 10^4$ and $5 \cdot 10^4$. Static morphing shows modest aerodynamic benefits with best increase of the L/D ratio of about 2%. However, dynamic morphing significantly reduces the size of flow separation therefore greatly increasing the L/D ratio. Bilgen et al. investigated the use of MFCs to change the wing camber for roll and pitch control of a remotely piloted micro-air-vehicle (MAV).¹⁷ The MAV was flown successfully and demonstrated sufficient roll control in flight as well as in the wind tunnel. It survived numerous crashes proving the durability of MFCs. Successively, Bilgen et al. investigated in detail the use of MFCs to change the camber of a symmetric airfoil.¹⁸ The progress of this research led to the fabrication and flight demonstration of a small aircraft with solid-state control surfaces.¹⁹ More recently, Bilgen et al. developed a novel design for a variable-camber airfoil employing a continuous inextensible surface with bonded MFC actuators which can achieve significant change in aerodynamic response.^{20,21} Moses et al. studied MFC actuators as a mean for reducing buffeting loads on a twin-tail fighter aircraft flying at high angles of attack.²² Wind-tunnel tests with open and closed-loop buffet alleviation have shown buffeting reductions of over 80%.

The main scope of this follow-on project is to explore the use of MFC actuators integrated to the upper and lower skins of a symmetric airfoil model for changing its shape to the degree required for tailoring a wing's performance. The mechanical design previously presented by Debiiasi et al.^{23,24} is applied in this study to both the upper and the lower surfaces on an airfoil. To some extent this work parallels those of Bilgen et al.¹⁸⁻²¹ However, it is based on a different mechanical design of the morphing wing whose structure is more similar to that of conventional wings, a desirable characteristics for practical implementation in aircraft.

II. Experimental Setup

A symmetric airfoil model has been fabricated for testing the shape changes of its upper and lower surfaces by MFC actuators, Figs. 2 and 3. The model chord c is 150 mm and its span s is 158 mm. The reference geometry for fabrication of the airfoil is the NACA 0015. However the actual fabricated model has maximum thickness of 21 mm without MFC actuation and thus the corresponding geometry is closer to that of a NACA 0014 airfoil. A 0.25 mm-thick carbon-fiber sheet, a material suitable for fabricating the skin of small aircraft, has been used for the upper and lower skins. A vacuum-bag was used to bond the MFC patches (Smart Material M-8557-P1) to the inner side of the skins, Fig. 3b). The skins deform inward when a positive voltage is applied to the MFCs, whereas they deform outward when a negative voltage is applied. Such deformations cause the skins to have small variations in the longitudinal direction which are accommodated by allowing them to slide in thin pockets located at the leading edge.

The MFC actuators are driven by a Smart Material HVA 1500/50-2 high-voltage amplifier which is designed to power a number of different piezo-actuators. This unit has a voltage gain of 200 V / V and a signal bandwidth from DC to 10 kHz depending on the load capacitance. It accepts input voltages in the range from -2.5 V to 7.5 V which are amplified to values of -500 V to 1500 V, the voltage range of the MFC actuators.

The aerodynamic characteristics of the model have been tested in the small, open-loop, subsonic wind tunnel of the NUS Temasek Laboratories, Fig. 4. The range of the wind-tunnel freestream velocity U_∞ is 2 to 35 m/s. Square test sections with width and height of 160 mm and different lengths can be connected to the exit of the wind-tunnel nozzle which has a 9.8:1 contraction ratio. The turbulence intensity level of the wind-tunnel freestream is less than 0.25%. The leading edge of the model was positioned 200 mm downstream of the nozzle. In this location the boundary-layer thickness of the empty test section is less than 3 mm for values of U_∞ between 10 to 20 m/s. The nominal velocity of the flow upstream of the model was obtained by measuring its total pressure with a pitot intake upstream of the nozzle (and downstream of the settling chamber meshes) and its static pressure with a tap located in the wall of the test section 120 mm downstream of the nozzle. The total and static pressure ports were connected to an Extech HD350 digital anemometer. This arrangement permitted controlling and maintaining the flow velocity within ± 0.1 m/s.

The deformation of the upper and lower skin with actuation of the MFCs was measured with a Micro-Epsilon optoNCDT 1710-50 laser displacement sensor. This unit has a measuring range between 550 and 600 mm with a resolution of 5 μm and an accuracy of 50 μm . The measuring range allows it to be placed outside the wind-tunnel thus enabling measurements of the skin deformation in the flow. These were acquired at 312.5 Hz simultaneously to the corresponding values of the actuation voltage.

The model was mounted on a turntable incorporating a balance. The turntable allows precise positioning (within $\pm 0.2^\circ$) of the angle of attack α of the model. The balance consists of a Gamma ATI SI-65-5 piezoelectric gauge. This unit can measure the forces and the moments along three perpendicular axes. We used two axes aligned with the streamwise and the vertical directions of the wind tunnel to measure the drag and the lift forces generated by the model. The third axis, coinciding with the axis of rotation of the turntable and aligned in the spanwise direction, passed through the airfoil mid-chord point ($c/2$) and was used to measure the pitching moment. The balance was factory calibrated and the corresponding conversion factors stored in the acquisition unit used with it such that the values of the forces and moments obtained are already corrected. The range (and accuracy) of the measured forces and moment are 65 ($\pm 1/80$) N and 5 ($\pm 8 \cdot 10^{-4}$) Nm, respectively. For each measurement, 2048 samples of the values of the forces and moment were acquired at 2 kHz and low-pass filtered at 10 Hz before averaging in order to remove the effect of small vibrations induced by the flow. Based on the angle of attack, the pitching moment about $c/4$ was calculated from the corresponding values of the lift, drag, and pitching moment about $c/2$. The maximum error for these quantities is 5%.

III. Results

Figure 5 shows lateral-view pictures of the model changing the shape of its upper and lower surfaces with static actuation in still air. Figure 5a) is the non-actuated model whose shape is similar to the NACA 0014 airfoil. Figure 5b) shows the outward deformation of the surfaces with the MFCs actuated at -500V which produces a shape similar to the NACA 0016 airfoil. Conversely, actuation at 1000V causes an inward skin deformation. This produces a thinner profile of unconventional flatter shape whose thickness is about 13% of the chord, Fig. 5c). Finally, actuation at different upper and lower skin voltages produces asymmetric profiles with non-zero curvature of the camber line. Figure 5d) shows such a profile obtained with upper-skin actuation at -500V and lower-skin actuation at 1500V. In this figure A and B indicate the points at $0.4 c$ from the leading edge of the model located on the upper and on the lower surface, respectively. The corresponding negative-cambered (i.e. upside-down) airfoil is simply

obtained by inverting the actuation voltages of the upper and of the lower skins. Other shapes, not shown here, can be obtained by adjusting the actuation voltages of the upper and of the lower skins within the range of values permissible for the MFCs.

Figure 6 illustrates the displacement in the n direction of the skin measured at $0.4 c$. Positive and negative values indicate outward and inward deformations, respectively. Figure 6a) shows the actuation voltage and the corresponding skin displacement in still air during one actuation cycle between -500 V and 1500 V. The voltage was kept constant for 0.5 s at the extremes of the voltage range. Points A and B in Figs. 6a) and 6b) match the corresponding points of Fig. 5d). Point A on the upper surface moved outward by about 1.5 mm relative to the non-actuated case of Fig. 5a) whereas point B on the lower surface moved inward by about 2 mm. Thus the thickness of the airfoil measured at $0.4 c$ decreased by only 0.5 mm whereas its camber increased by 3.5 mm which corresponds to a 2.3% c positive camber. A hysteresis loop is obtained by plotting the skin displacement as a function of the actuation voltage. This is an undesirable but typical behavior due to the piezo-ceramic bimorph nature of the MFC actuators.¹⁸ Figure 6b) shows five such loops which overlap quite well indicating good repeatability of the displacement with actuation. The arrows in the figure indicate the loop path.

Figures 6c) and 6d) show analogous data for the airfoil aerodynamically loaded at $\alpha = 0^\circ$ in a $U_\infty = 15$ m/s flow. Compared to the still-air measurements, a small positive displacement of the skin is observed with actuation at -500 V which is attributed to the low pressure on the upper surface. Similarly, the skin tends to be slightly pulled out when moving from the inward to the outward position (upward path of the hysteresis loop). However, the skin behaves as in the still-air case when moving from the outward to the inward position (downward path of the hysteresis loop) indicating that the actuators are actually capable of contrasting the aerodynamic loads as required. Similar results (not shown here) have been obtained at other angles of attack.

Wind-tunnel tests were performed at freestream velocities up to 15 m/s for values of the angle of attack ranging between -15° to 15° . In this range of velocities and angles of attack, the upper and lower skins of the model did not exhibit any vibration or anomalous deformation both without and with actuation. The response to actuation of the skins was similar to that observed in still air, as shown above.

Figure 7 compares the aerodynamic characteristics of the airfoil model without actuation and with actuation of the skins at -500 V and 1500 V to obtain positive and negative-cambered airfoil shapes as in Fig. 5d). The data, obtained at $U_\infty = 15$ m/s for α ranging between -15° to 15° , are not corrected for the effects of tunnel blockage. Larger values of the angle of attack are not considered since these would be significantly affected by the blockage of the model (whose chord is comparable to the height of the wind-tunnel test section). At this velocity, the Reynolds number Re_c based on the chord of the model is about $150,000$ and thus the flow around the model is laminar. The lift coefficient of the three configurations is shown in Fig. 7a) for the positive range of the angles of attack. As expected, increasing the camber produces higher lift. At higher angles of attack the negative-cambered airfoil suffers a loss of lift due to flow separation. The values for $\alpha < 0^\circ$ can be obtained by mirroring the data of Fig. 7a) about the two axes in which case the data of the positive-camber case would be the mirrored data of the negative-camber case, and vice-versa. By changing the voltage of the skins between the extreme values of the positive and negative-camber cases, one can obtain intermediate shapes between these and, accordingly, values of the lift coefficient comprised between the higher and the lower curves of Fig. 7a). Analogous considerations hold also for the successive figures. Figure 7b) shows that, as expected, the positive-cambered airfoil suffers less drag at positive angles of attack. The corresponding values of the lift over drag ratio are shown in Fig. 7c) clearly showing that a more efficient configuration for cruise conditions can be obtained by increasing the camber of the airfoil. A typical application of symmetric airfoils is in highly maneuverable aircraft. The lift-drag polars in Fig. 7d) indicate that such an aircraft with a wing capable of adopting positive and negative-cambered airfoil shapes would achieve the required lift with minimum drag both in normal or inverted flight and in any other in-between flight condition. Figures 7e) and 7f) show the pitching-moment coefficient about $c/4$ and the non-dimensional chordwise position of the center of pressure as a function of the angle of attack, respectively. We can see from these figures that changing the shape of the airfoil can be used to tailor the location of its center of pressure, and thus the stability of the aircraft, without adversely affecting its pitching moment.

The data in Fig. 7 show that the shaping of the upper and lower surfaces by MFC actuators can be useful for increasing the aerodynamic performance of a symmetric airfoil which, being simpler to design and construct, is the type studied in this work. However, the technique presented here is not limited to symmetric airfoils. In principle, the shaping of the upper and lower surfaces by MFC actuators can be useful for tailoring and improving the aerodynamic performance of any type of airfoil. In particular, this technique could be very beneficial to broaden and stabilize the useful aerodynamic envelope of high-performance airfoils that quickly deteriorate their characteristics at off-design conditions.

IV. Conclusion

A symmetric airfoil model has been designed and constructed that has flexible upper and lower skins whose shapes can be changed by macro fiber composite (MFC) actuators bonded to their inner sides. These piezoelectric actuators are very thin, light, robust, and have low power consumption. In the design discussed, they become an integral part of the skin of the model. Without actuation the model has a shape similar to that of the NACA 0014 airfoil. Different symmetric and non-symmetric airfoil shapes can be obtained by changing the actuation voltage of the upper and of the lower skins within the range allowed for the MFC actuators. The aerodynamically loaded skins did not show any vibration or anomalous deformation and maintained a response to the actuation comparable to that observed in still air. The undesirable but typical hysteresis of the MFC actuators can pose some difficulties in achieving a specified airfoil shape. Closed-loop control should be used in practical applications to overcome this problem and to actuate the skins to a desired aerodynamic shape. The aerodynamic characteristics of the model have been measured with a force balance in a wind tunnel. The results obtained clearly indicate that it is possible to increase the aerodynamic performance of a symmetric airfoil by using MFC actuators to change the shape of its upper and lower surfaces. In principle this technique should be useful for tailoring and improving the aerodynamic performance of other types of airfoil as well. To prove this, new asymmetric airfoil models will be fabricated and tested in the future.

References

- ¹ Reich, G. W., Bowman, J. C., and Sanders, B., "Large-Area Aerodynamic Control for High-Altitude Long- Endurance Sensor Platforms," *Journal of Aircraft* Vol. 42, No. 1, pp. 237.
- ² Maute, K. K., and Reich, G. W., "Integrated Multidisciplinary Topology Optimization Approach to Adaptive Wing Design," *Journal of Aircraft* Vol. 43, No. 1, pp. 253.
- ³ Austin, F., Rossi, M. J., Van Nostrand, W., Knowles, G., and Jameson, A., "Static shape control for adaptive wings," *AIAA Journal* Vol. 32, No. 9, pp. 1895-1901.
- ⁴ Laxminarayana Saggere, and Sridhar Kota, "Static Shape Control of Smart Structures Using Compliant Mechanisms," *AIAA Journal* Vol. 37, No. 5, pp. 572.
- ⁵ Secanell, M., Suleman, A., and Gamboa, P., "Design of a Morphing Airfoil Using Aerodynamic Shape Optimization," *AIAA Journal*, Vol. 44, No. 7, pp. 1550-1562.
- ⁶ Siclari M. J., Van Nostrand, W., and Austin, F., "The design of transonic airfoil sections for an adaptive wing concept using a stochastic optimization method," AIAA Paper 96-0329.
- ⁷ Martins, A. L., and Catalano, F. M., "Drag optimization for transport aircraft Mission Adaptive Wing," *Journal of the Brazilian Society of Mechanical Sciences and Engineering* Vol. 25, No. 1, Jan./Mar. 2003.
- ⁸ Hubbard, J. E. Jr., "Dynamic Shape Control of a Morphing Airfoil Using Spatially Distributed Transducers," *Journal of Guidance, Control, and Dynamics*, Vol. 29, No. 3, pp. 612-616.
- ⁹ Munday, D., Jacob, J., and Huang, G., "Active Flow Control of Separation on a Wing with Oscillatory Camber," AIAA Paper 2002-0413, 40th AIAA Aerospace Sciences Meeting & Exhibit, Jan. 2002.
- ¹⁰ Munday, D., and Jacob, J., "Active Control of Separation on a Wing with Oscillating Camber," *Journal of Aircraft*, Vol. 39, No. 1, 2002, pp. 187-189.
- ¹¹ Munday, D., Jacob, J., Hauser, T., and Huang, G., "Experimental and Numerical Investigation of Aerodynamic Flow Control Using Oscillating Adaptive Surfaces," AIAA Paper 2002-2837, 1st AIAA Flow Control Conference, June 2002.
- ¹² Ehlers, S. M., and Weisshaar, T. A., "Static aeroelastic control of an adaptive lifting surface," *Journal of Aircraft* Vol. 30, No. 4, pp. 534-540.
- ¹³ Rocha, J., Moniz, P. A., Costa, A. P., and Suleman, A., "On Active Aeroelastic Control of an Adaptive Wing Using Piezoelectric Actuators," *Journal of Aircraft* Vol. 42, No. 1, pp. 278-281.
- ¹⁴ Weisshaar, T. A., and Duke, D. K., "Induced Drag Reduction Using Aeroelastic Tailoring with Adaptive Control Surfaces," *Journal of Aircraft* Vol. 43, No. 1, pp. 157-164.
- ¹⁵ Gern, F., Inman, D. J., and Kapania, R. K., "Computation of Actuation Power Requirements for Smart Wings with Morphing Airfoils," *AIAA Journal* Vol.43, No.12, pp. 2481-2486.
- ¹⁶ Pinkerton, J. L., and Moses, R. W., "A Feasibility Study To Control Airfoil Shape Using THUNDER," NASA Technical Memorandum 4767.
- ¹⁷ Bilgen, O., Kochersberger, K. B., Diggs, E. C., Kurdila, A. J., and Inman, D. J., "Morphing Wing Micro-Air-Vehicles via Macro-Fiber-Composite Actuators," AIAA Paper 2007-1785, *48th AIAA/ASME/ASCE/AHS/ASC Structures, Structural Dynamics, and Materials Conference*, Honolulu, Hawaii, Apr. 23-26, 2007.
- ¹⁸ Bilgen, O., Kochersberger, K. B., Inman, D. J., and Ohanian, O. J. III, "Novel, Bidirectional, Variable-Camber Airfoil via Macro-Fiber Composite Actuators," *Journal of Aircraft* Vol. 47, No. 1, pp. 303-314.
- ¹⁹ Bilgen, O., Butt, L. M., Day, S. R., Sossi, C. A., Weaver, J. P., Wolek, A., Mason, W. H., and Inman, D. J., "A Novel Unmanned Aircraft with Solid-State Control Surfaces: Analysis and Flight Demonstration," AIAA Paper 2011-2071, *52nd AIAA/ASME/ASCE/AHS/ASC Structures, Structural Dynamics, and Materials Conference*, Denver, Colorado, Apr. 4-7, 2011.
- ²⁰ Bilgen, O., Saavedra Flores, E. I., and Friswell, M. I., "Implementation of a Continuous-Inextensible-Surface Piezocomposite Airfoil," AIAA Paper 2012-1902, *53rd AIAA/ASME/ASCE/AHS/ASC Structures, Structural Dynamics, and Materials Conference*, Honolulu, Hawaii, Apr. 23-26, 2012.
- ²¹ Bilgen, O., Landman, D., and Friswell, M. I., "Low Reynolds Number Behavior of a Solid-State Piezocomposite Variable-Camber Wing," AIAA Paper 2013-1515, *54th AIAA/ASME/ASCE/AHS/ASC Structures, Structural Dynamics, and Materials Conference*, Boston, Massachusetts, Apr. 8-11, 2013.
- ²² Moses, R. W., Pototzky, A. S., Henderson, D. A., Galea, S. C., Manokaran, D. S., Zimcik, D. G., et al., "Actively Controlling Buffet-Induced Excitations," report RTO-MP-AVT-123, Symposium on Flow Induced Unsteady Loads and the Impact on Military Applications, Apr. 2005.
- ²³ Debiasi, M., Bouremel, Y., Khoo, H. H., Luo, S. C., and Tan, E. Z., "Shape Change of the Upper Surface of an Airfoil by Macro Fiber Composite Actuators", AIAA Paper 2011-3809, *29th AIAA Applied Aerodynamics Conference*, Honolulu, HI, June 2011.
- ²⁴ Debiasi, M., Bouremel, Y., Khoo, H. H., and Luo, S. C., "Deformation of the Upper Surface of an Airfoil by Macro Fiber Composite Actuators", AIAA Paper 2012-3206, *30th AIAA Applied Aerodynamics Conference*, New Orleans, Louisiana, June 2012.



Figure 1. Macro fiber composite (MFC) actuator [image courtesy of Smart Material Corp.].

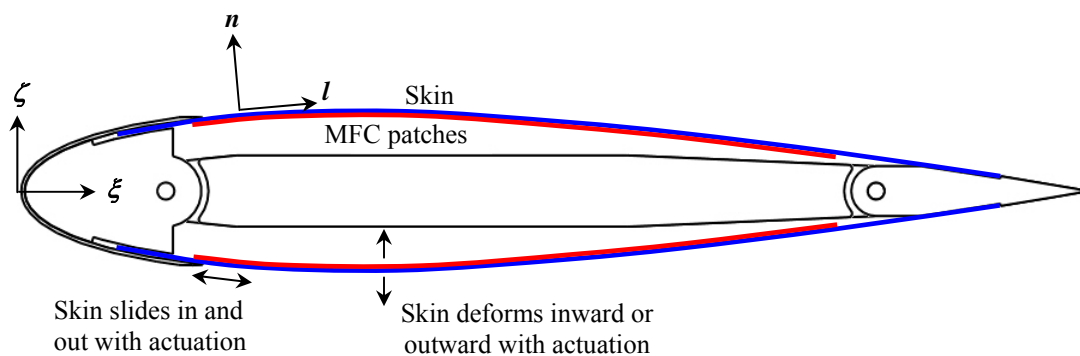


Figure 2. Schematic diagram of the airfoil model with upper and lower-surface actuation by MFC patches.

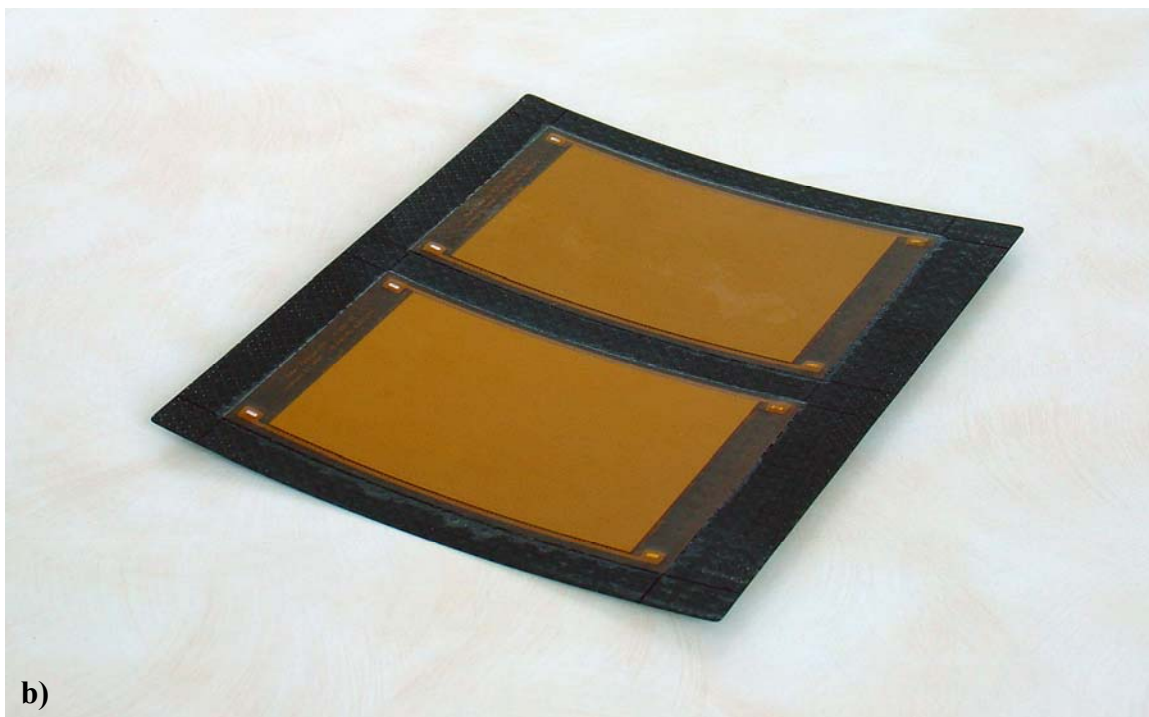
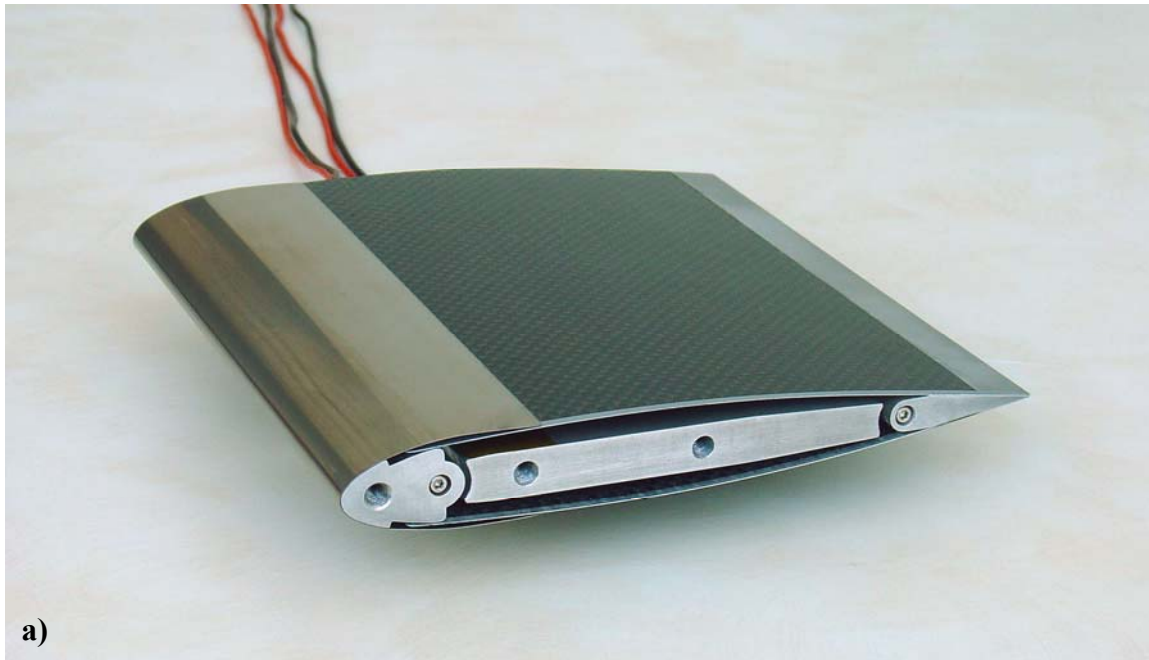


Figure 3. Airfoil model for testing: a) assembled model; b) inner side of a carbon-fiber skin with MFC patches.

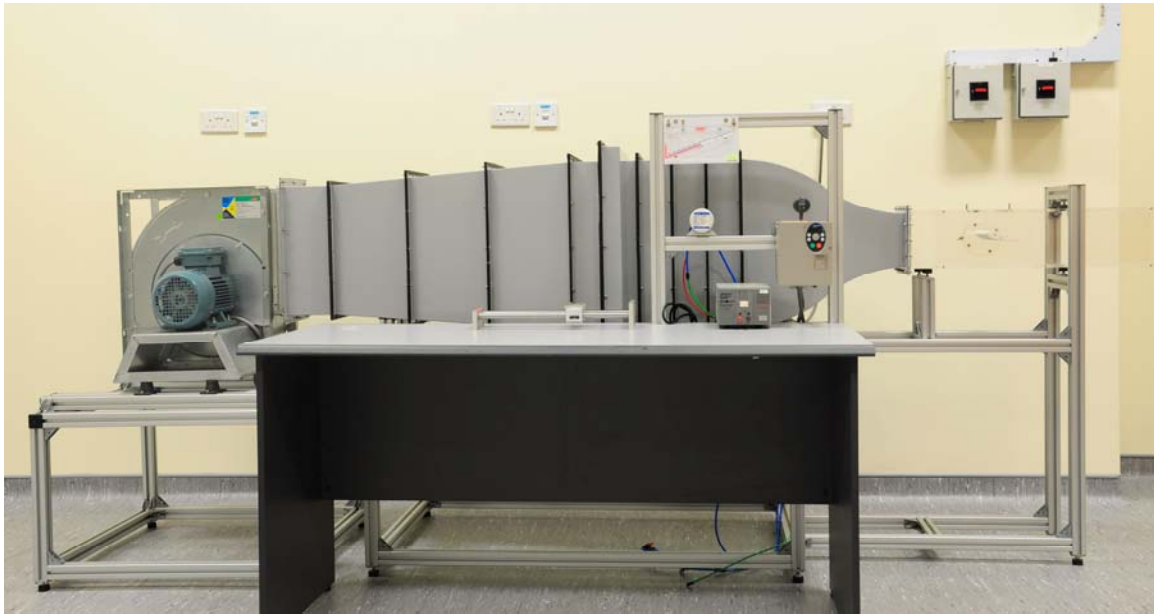


Figure 4. Small, open-loop, subsonic wind tunnel of the NUS Temasek Laboratories.

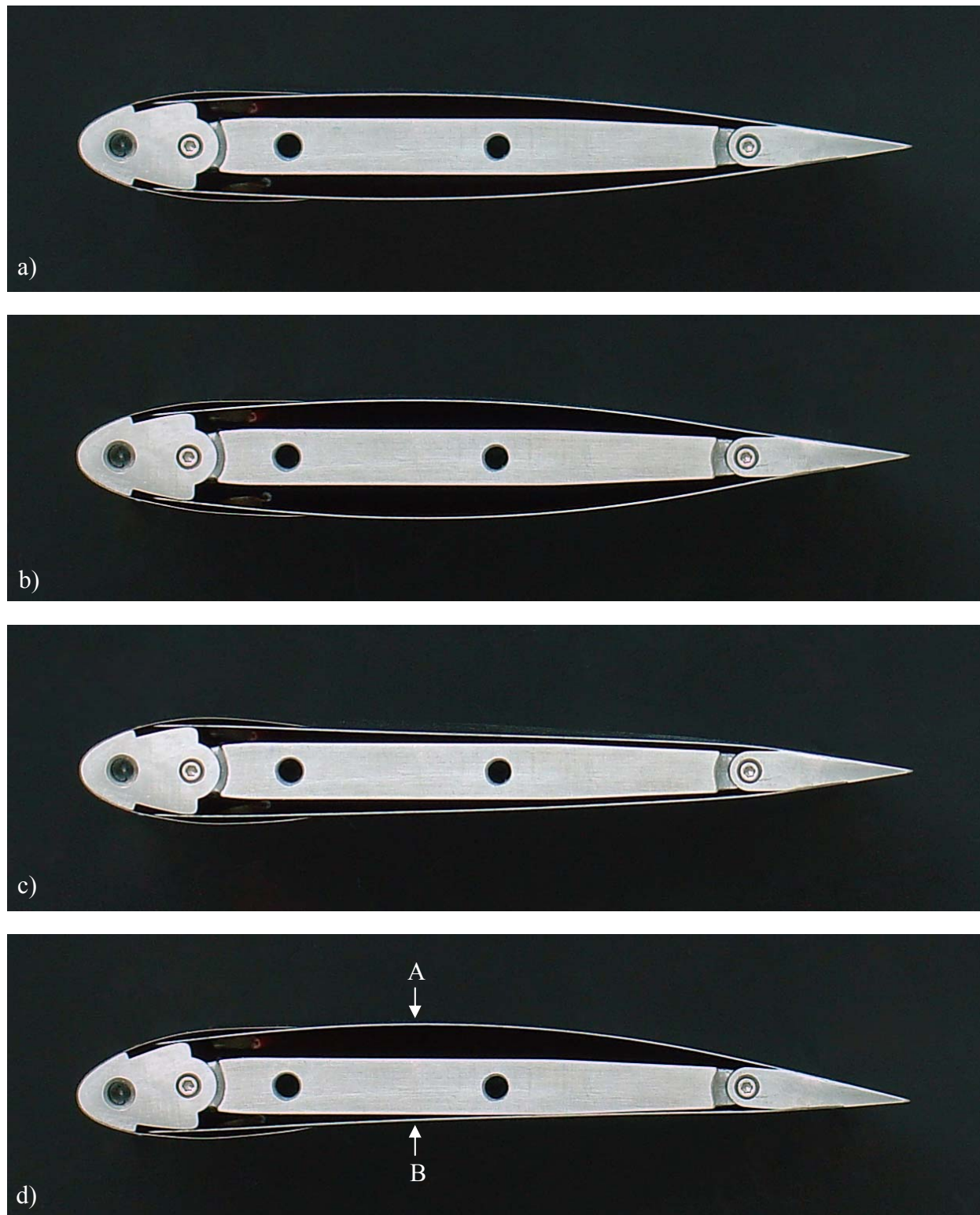


Figure 5. Lateral view of the airfoil model: a) without actuation (shape similar to a NACA 0014 airfoil); b) with actuation of both the upper and lower skins at -500 V (shape similar to a NACA 0016 airfoil); c) with actuation of both the upper and lower skins at 1500 V (flatter shape); d) with upper-skin actuation at -500 V and lower-skin actuation at 1500 V.

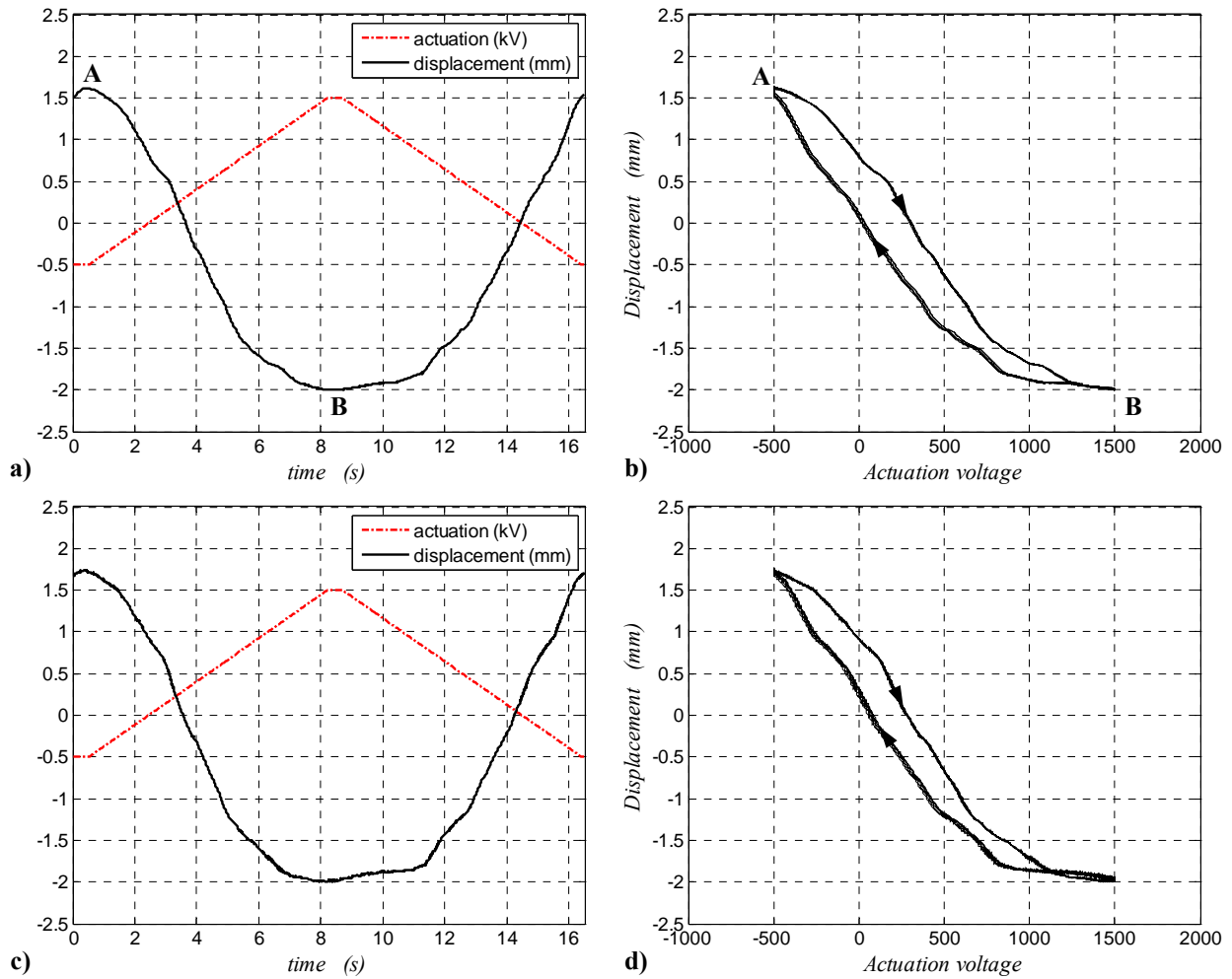


Figure 6. Displacement of the skin at 0.4 c: a) actuation and displacement, and b) hysteresis loop without flow; c) actuation and displacement, and d) hysteresis loop with aerodynamic load at $\alpha = 0^\circ$ in a $U_\infty = 15$ m/s flow.

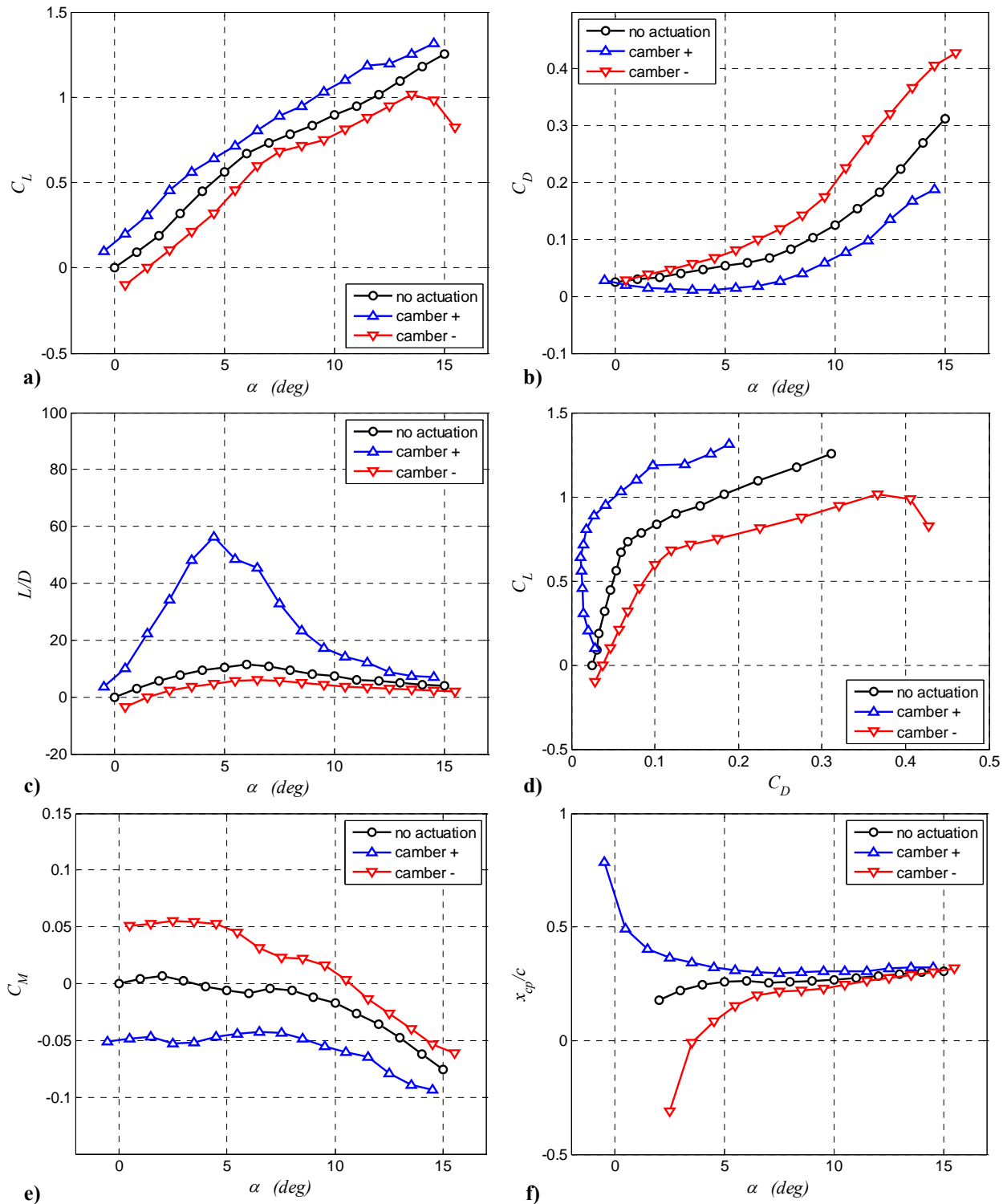


Figure 7. Aerodynamic characteristics of the airfoil model without and with actuation: a) lift coefficient; b) drag coefficient; c) lift over drag ratio; d) lift-drag polar; e) pitching-moment coefficient about $c/4$; f) non-dimensional chordwise position of the center of pressure.